Macromolecules
ARTICLE

Macromolecules **2009**, *42*, 8211–8217 **8211**
DOI: 10.1021/ma901420h

Self-Assembly of Poly(3-hexylthiophene)-*block*-polylactide Block Copolymer and Subsequent Incorporation of Electron Acceptor Material

Ioan Botiz and Seth B. Darling*

Center for Nanoscale Materials, Argonne National Laboratory, 9700 South Cass Avenue, Argonne, Illinois 60439

Received July 1, 2009; Revised Manuscript Received August 5, 2009

ABSTRACT: It is commonly accepted that in order to develop high-performance organic and/or hybrid organic−inorganic solar energy devices, it is necessary to use, among other components, an active donor−acceptor layer with highly ordered nanoscale morphology. In an idealized morphology, the effectiveness of internal processes including exciton generation and separation and charge carrier migration is optimized, leading to an efficient conversion of photons to electricity. With this idea in mind, we have rationally designed and developed an ordered nanoscale morphology consisting of self-assembled poly(3-hexylthiophene) donor domains of molecular dimension, each of them separated by fullerene C_{60} hydroxide acceptor domains. A poly(3-hexylthiophene)-*block*-poly(L-lactide) block copolymer was used as a structure-directing agent to pattern active material into ordered nanostructures. Using this intimate morphological control, one can begin to probe structure−property relationships with unprecedented detail with the ultimate goal of maximizing the performance of future organic/hybrid photovoltaic devices.

Introduction

The ever-growing societal demand for energy—in particular from renewable resources—has encouraged the scientific community to explore various methodologies for converting sunlight to electricity. The result of decades of research in this field can be seen in today's inorganic solar energy device technology, with multijunction cells exhibiting greater than 40% efficiency.[1] Though they are well-suited to some small markets, these technologies are currently too expensive to implement on a global scale, so scientists are directing fresh attention toward new generations of organic and/or hybrid low-cost photovoltaic (PV) devices.[2−13] Today, the demonstrated efficiency of such PV energy devices is limited to a few percent, but these efficiencies are far short of the thermodynamic limit.

Efficient conversion of photons to electricity in organic and hybrid materials depends on optimization of factors including light absorption,[9,14] exciton separation,[15−17] and charge carrier migration.[10,14] Various PV device concepts have been developed, including polymer-based solar cells. The most efficient such devices are made by blending a semiconducting polymer either with fullerenes,[5,8,18−20] other polymers,[21−23] or nanocrystals.[24−26] One clear conclusion that appears continuously when dealing with polymer-based solar energy devices is that donor−acceptor bulk heterojunction (BHJ) devices target key internal processes, but disorder on the nanoscale results in inefficiencies due to exciton recombination and poor mobility (the objective of BHJ design is to efficiently dissociate photogenerated excitons[15]). Today, it is accepted that, in order to develop high-performance organic and/or hybrid organic−inorganic solar energy devices, it is necessary to control the active layer morphology on the nanoscale.[27−31]

By drawing on the flexibility of modern synthetic chemistry, one can design new organic/inorganic materials with novel properties aimed at transcending the limitations associated with traditional BHJ cells. One promising approach is to design block copolymers possessing one or more optoelectronic active blocks.[32−39] These copolymers can undergo, under certain conditions, a microphase separation process and can lead to ordered morphologies on surfaces[40] characterized by nanostructured domains of characteristic distance (tuned by the polymer block lengths). In this way, one can utilize rationally designed self-assembly to control the morphology at the nanoscale and thereby engineer enhanced effectiveness of internal processes, ultimately improving the performance of PV devices.[41]

The goal of the work presented here is to experimentally implement the idea of morphological control using common PV active component materials: poly(3-hexylthiophene) and C_{60}. While the standard approach is to mix these two compounds and manipulate processing conditions to try to optimize nanoscale phase separation in the BHJ layer, we have designed a novel fabrication process that relies on self-organization to generate idealized morphology. The starting material is a poly(3-hexylthiophene)-*block*-poly(L-lactide) (P3HT-*b*-PLLA) linear diblock copolymer (Figure 1a), similar to a polymer recently reported by Hillmyer et al.[42] The molecular weights of the two blocks were selected to encourage self-assembly into a lamellar structure. P3HT is a semiconducting polymer. Covalently linking to PLLA, as opposed to a second conjugated polymer, permits relatively facile synthesis; an additional role of the PLLA is described below. The P3HT-*b*-PLLA is designed to be used both as an optoelectronically active material *and* as a structure-directing agent to pattern active material into ordered nanostructures (schematically depicted in Figure 1b). Specifically, the P3HT block is attractive due to its large charge carrier mobility[43] and band gap in the visible region of the spectrum.[44] The characteristic periodicity, which will eventually translate into the donor−acceptor length scale, for P3HT-*b*-PLLA was designed to be ∼15 nm, i.e., comparable to the exciton diffusion length throughout the active layer.[27,45]

An essential advantage of using P3HT-*b*-PLLA is the fact that the coiled PLLA block is biodegradable.[46] Therefore, once the

*Corresponding author. E-mail: darling@anl.gov.

Published on Web 08/14/2009

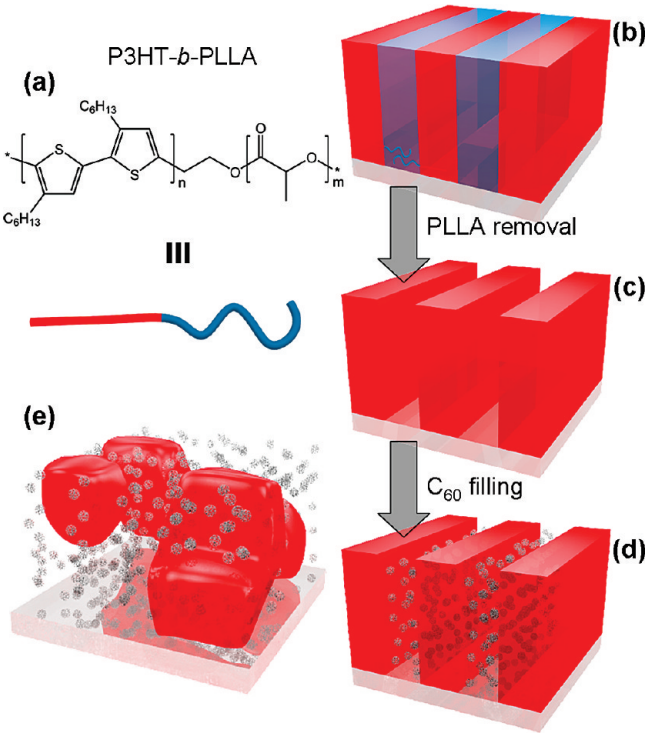

Figure 1. (a) Chemical structure of P3HT-*b*-PLLA linear diblock copolymer and its schematic representation. (b) Ordered nanoscale morphology consisting of lamellae oriented perpendicular to the substrate and expected to be found in thin solid films of P3HT-*b*-PLLA. (c) Ordered P3HT donor domains of molecular dimension expected to be obtained after removal of biodegradable PLLA block. (d, e) Comparison of an ordered nanoscale morphology consisting of self-assembled P3HT donor domains, each of them separated by C_{60} acceptor domains (d) and a less ordered morphology obtained when simply blending both P3HT donor homopolymer and C_{60} acceptors (e).

microphase separation process (between the two incompatible blocks: P3HT and PLLA) is complete and the ordered nanoscale morphology is obtained, the PLLA block can be readily removed.[42] The expected morphology at this point is schematically depicted in Figure 1c. The removal of PLLA opens new possibilities. For example, we can use the former PLLA domains (now empty) as vessels for an acceptor material like fullerene hydroxide (C_{60}). The more traditional form of C_{60}, [6,6]-phenyl-C_{61}-butyric acid methyl ester (PCBM), is not suitable in this process because organic solvents would destroy the nanostructured P3HT template. Such an approach should directly lead to the new donor−acceptor ordered nanoscale morphology schematically depicted in Figure 1d. This morphology, consisting of alternating donor−acceptor nanostructured domains, is expected to enhance the effectiveness of internal processes compared to a less ordered BHJ morphology (Figure 1e) obtained when simply mixing P3HT homopolymer with PCBM. The disordered BHJ includes some domains much larger than the exciton diffusion length, resulting in inactive volumes, as well as many domains that do not contain continuous pathways to the electrodes, which results in poor charge carrier mobility and, hence, decreased efficiency. Recent reports have indicated that internal efficiencies can approach unity when processing conditions are fully optimized;[47] however, the ordered BHJ approach enabled through the utilization of block copolymers provides a pathway for systematic studies of structure−property relationships. Analogous methodologies could also be applied to other donor and acceptor materials to optimize light absorption and solar cell parameters such as open-circuit voltage.

Experimental Methods

The P3HT-*b*-PLLA linear diblock copolymer was purchased as a custom synthesis from Polymer Source, Inc., and used without further purification. The number-average molecular weight was $M_n = 3300$ for P3HT and $M_n = 4100$ for PLLA. The polydispersity index (M_w/M_n, PDI) was 1.28, as measured by size exclusion chromatography. Fullerene C_{60} hydroxide [chemical structure: $C_{60}(OH)_{22-26}$] was purchased from Materials Technologies Research, Ltd. This acceptor material is water-soluble at pH ≥ 8. Differential scanning calorimetry (DSC) data were obtained with a Mettler-Toledo 823 calorimeter. Thin solid films with an average thickness of ~70 nm (measured by ellipsometry and profilometry) were obtained by spin-casting chloroform polymer solution onto various solid substrates: (a) SiO_2, (b) ITO-covered glass, or (c) PEDOT:PSS-covered ITO/glass. The latter two substrates were selected based on their importance in the fabrication of organic PV devices. Spin conditions were 2000 rpm for 60 s from a 15 mg/mL solution. Solvent annealing was performed by placing the sample in a sealed bell jar with a saturated chloroform vapor. The sample was removed by venting the vapor over the course of ~15 s. The surface of the thin films was characterized in detail by tapping-mode atomic force microscopy (Nanoscope V, Veeco). Electron micrographs were obtained with a 300 kV FEI Tecnai F30 transmission electron microscope (TEM) with a high-resolution CCD camera. To verify the continuity of the lamellae through the film, TEM samples were prepared on silicon nitride membrane substrates and stained using RuO_4 vapor to enhance contrast between the two polymer blocks. ATR FT-IR spectra were recorded using a Vertex 70 spectrometer from Bruker and a 20× ATR objective (Ge crystal). The etching process used to selectively remove the biodegradable PLLA block consisted of treatment of thin polymer films in 0.5 M NaOH solution (60:40 v/v water/methanol). Thin films were submerged in NaOH solution for different times and then either carefully rinsed with water in order to remove degraded PLLA fragments and Na or transferred consecutively to a series of beakers containing dry, absolute ethanol to execute a thorough solvent exchange. After rinsing, thin films were dried overnight at room temperature. Fullerene filling was achieved by dip-coating for 72 h in an aqueous solution of 15 mg/mL concentration. X-ray diffraction data were obtained using a Bruker D8 Discover analytical X-ray system in a grazing incidence geometry (θ_i = 0.17). Emission photoluminescence spectra were recorded using a Perkin-Elmer LS-55 luminescence spectrometer with a 250 nm/min scan rate and excitation wavelength of 500 nm.

Results and Discussion

Figure 2 shows the resulting morphology obtained after spin-casting P3HT-*b*-PLLA chloroform solution on the three different solid substrates. In all cases, we observe a morphology comprised of periodic parallel stripe domains. Domains of lighter color correspond to the P3HT block while the darker domains are the PLLA amorphous block, suggesting a lamellar structure with the alternating domains oriented perpendicular to the substrate. Similar elongated structures have been observed in low molecular weight P3HT homopolymer films;[48] domains of aligned structures in these published AFM images (M_n of 3.2K) exhibit a periodicity of ~8 nm, or about half that seen in Figure 2. The molecular weight of this homopolymer corresponds well with the molecular weight of the P3HT block in the copolymer, suggesting that the difference in periodicity can be attributed to the PLLA blocks that are interspersed between the P3HT domains due to lamellar microphase separation. While AFM probes the top surface of the polymer film, there are three reasons to believe the perpendicular morphology extends down from the free interface to the substrate. The first is that a number of groups have completed rigorous structural studies on related rod−coil block copolymers, including one comprised of the same block materials

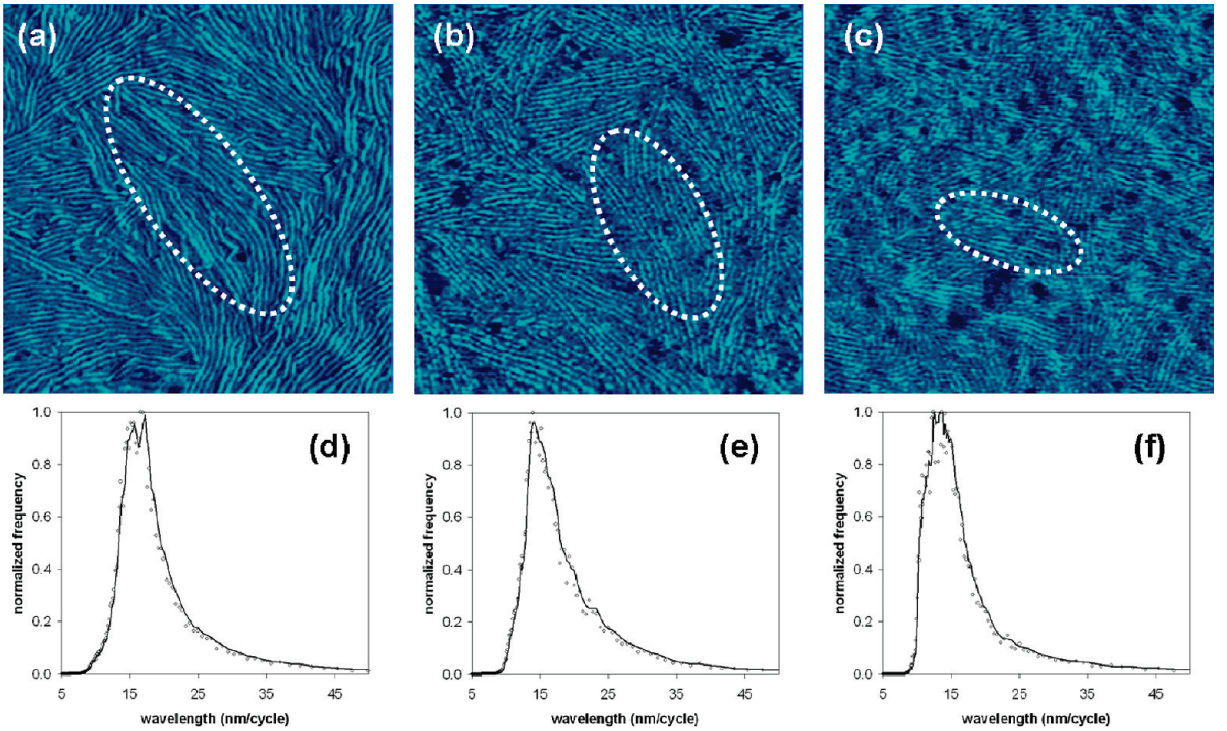

Figure 2. TM-AFM phase images showing ordered morphologies obtained by spin-casting of P3HT-*b*-PLLA on various substrates: (a) SiO_2 (polymer film thickness was 71 ± 3 nm); (b) ITO-covered glass (polymer film thickness was 69 ± 3 nm); (c) PEDOT:PSS-covered ITO (polymer film thickness was 72 ± 3 nm, PEDOT:PSS film thickness was 60 ± 5 nm). (d), (e), and (f) show the corresponding PSDs. The AFM image in (b) was taken after annealing in chloroform vapor for 90 h. All films were spin-cast from chloroform solution. Size of all AFM images is 1 μm^2.

and characterized with wide-angle X-ray scattering with evidence for lamellar structure.[42] In the context of comparison with these studies, it is important to note that PLLA has been reported to be semicrystalline,[49] and we do observe a small signature for a melting transition at $T \sim 170$ °C in DSC scans of the P3HT-*b*-PLLA block copolymer (Figure S-1). Crystallinity of the PLLA block may play some role in these films, but X-ray diffraction data have shown no sign of significant PLLA crystallization. Using TEM and small-angle X-ray scattering, Dai et al. have shown that P3HT-*b*-P2VP films, with rod volume fraction similar to that in the P3HT-*b*-PLLA material studied here, form continuous perpendicular lamellae.[50] The lateral domains they observe closely resemble those seen in Figure 2, yet the transmission aspect of their electron micrographs shows clearly that the domains persist from the top surface to the substrate. Hadziioannou et al., relying on both AFM and TEM data, the former also reminiscent of Figure 2, have reported perpendicular lamellae for the rod−coil polymer PPV-*b*-PBA.[51] Yet another recent example comes from Segalman et al.,[52] who have studied the rod−coil PPV-*b*-PI using electron diffraction, X-ray scattering, and AFM; they also report perpendicular morphology for volume fractions in the range of our material. In addition to this collection of results in the literature, there is a second reason to conclude that the perpendicular morphology extends throughout the film. The alternative possibility is that we have perpendicular lamellae at the free interface and parallel lamellae underneath. Indeed, such a mixed structure has been reported[52] for rod volume fractions significantly higher than in the system now under investigation. Aside from the fact that this structure is only seen when the rod block is much longer than the coil block, a case which does not apply here, if such an arrangement did exist in P3HT-*b*-PLLA, the film would not survive the NaOH treatment that removes the PLLA domains. Removal of PLLA domains oriented parallel to the substrate would delaminate the entire film. The fact that a nanostructured polymer film is still observed

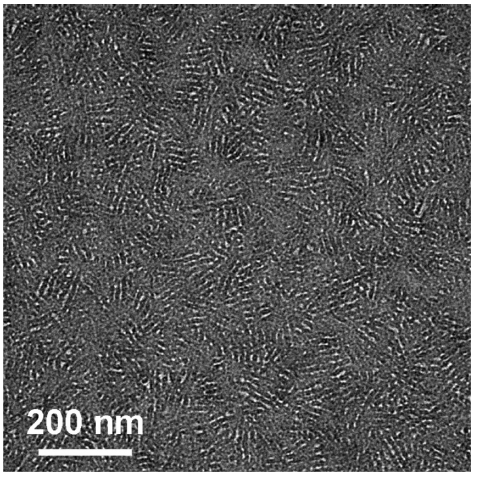

Figure 3. TEM image showing P3HT-*b*-PLLA lamellae in a film spin-cast from chloroform solution on a Si_3N_4 membrane substrate. This film has not been thermally or solvent annealed. Polymer film was stained by exposure to RuO_4 vapor to obtain contrast. This stain is expected to preferentially attack the thiophene rings of P3HT, making it appear darker in the image.

following NaOH treatment precludes the possibility of large areas populated by the parallel morphology. Third, TEM data presented in Figure 3, which represent a view through the full film thickness, exhibit structures similar to those observed on the top surface with AFM.

Characteristic locally ordered domains of stripes, which extend for several lamellar periods, are designated in Figure 2 by elliptical dotted shapes. Each of these aligned domains exhibit an orientation equivalent to the orientation of the substituent stripes. The diminished long-range ordering on indium tin oxide (ITO) and poly(3,4-ethylene dioxythiophene)−poly(styrenesulfonate)

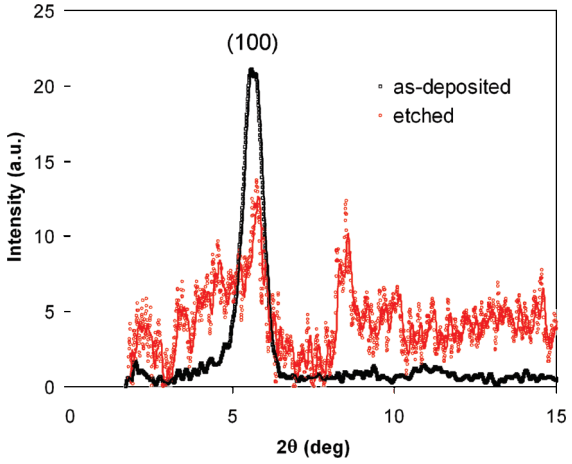

Figure 4. XRD spectra of P3HT-*b*-PLLA film on SiO_2 before and after NaOH etching. The (100) peak just above 5° corresponds to crystalline vertical stacking of P3HT chains.

(PEDOT:PSS)-covered ITO with respect to silicon oxide (SiO_2) is attributable to the lower surface roughness of the latter (0.5 nm vs ~5 nm rms roughness). For solar cell applications, in which electrodes are situated on the substrate and on top of the active layer, order along the vertical direction is essential for efficient charge carrier migration while order in the plane of the film is much less important. Analyzing the atomic force microscopy (AFM) images and their corresponding power spectral densities (PSD), we have found that the characteristic distances (17 ± 3 nm for SiO_2 and 16 ± 3 nm for both ITO and PEDOT:PSS/ITO, respectively) correspond well with the molecular length scale (~15 nm).

Comparing the results obtained for all three substrates, we have concluded that there is an influence of the substrate on the resulting surface morphology. When a SiO_2 substrate is used, the film morphology displays longer correlation lengths, i.e., better long-range in-plane order, compared to the cases of ITO and PEDOT:PSS. The ordered nanoscale morphology shown in Figure 2b (ITO substrate) was obtained after solvent annealing in chloroform vapor for 90 h (similar annealing has no apparent effect on the film structure for the other substrates studied). Before annealing, the parallel stripes could not be clearly visualized by AFM, indicating a less ordered initial morphology. In either case, ordered lamellae are readily achieved with minimal effort. In addition to characterizing the lateral domain morphology with microscopy, the molecular order in the plane perpendicular to the substrate was also probed with X-ray diffraction (XRD, Figure 4). The as-deposited block copolymer film exhibits a strong (100) diffraction peak at $2\theta \approx 5.4°$, which corresponds to crystalline vertical stacking of the P3HT chains.[53] Not only do these data indicate ordering that is known to possess good hole mobility, but they also provide further evidence for the lamellar phase morphology. This result represents the first step of the self-assembly methodology built on the rationally designed block copolymer P3HT-*b*-PLLA.

Once the ordered nanoscale morphology is obtained, there is no need for the PLLA block, which was used to simply direct structure formation by microphase separation, to remain. The goal is to create a donor−acceptor ordered nanoscale morphology. Therefore, the PLLA block was removed by employing an etching process. We have introduced our nanostructured films (69 ± 3 nm thickness) in 0.5 M NaOH solution for different periods of time. We have employed the attenuated total reflectance (ATR) Fourier-transform infrared (FT-IR) technique to monitor the etching of the PLLA block. The results are summarized in Figure 5a. The first spectrum (black line on top) was taken for a thin film of P3HT homopolymer to serve as a reference with no PLLA content. The rest of the spectra were recorded for structured films of P3HT-*b*-PLLA which were etched for times varying between 0.25 and 120 h. An analysis of ATR FT-IR spectra shown in Figure 5a reveals that several peaks (around 1050, 1095, 1135, 1195, 1270, 1450, and 1765 cm^{-1}, respectively) decreased with etching time and completely disappeared after 3 days of etching. According to the literature,[46] these peaks were assigned to the different stretching vibrations of PLLA block components. Figure 5b contains an illustrative example of the decrease of a PLLA peak area (1765 cm^{-1}; C═O stretch) with increasing etching time. These results demonstrate that, in order to completely remove the PLLA block, between 48 and 72 h of etching is necessary (for this particular film thickness).

AFM imaging was used to obtain complementary information to the ATR FT-IR spectra. Figure 5c shows the film morphology after removal of PLLA. These data display alternating dark features (corresponding to former locations of PLLA) and light features representing the P3HT nanostructured material. Whereas the measured depths of the trenches are only ~6 nm, the actual depths are likely larger; limitations associated with the profile of the AFM tip preclude accurate measurements of this topography. On the basis of the spectroscopy, it appears that all of the PLLA (and none of the P3HT) has been removed, suggesting that the actual depth of the trenches is comparable to the initial polymer film thickness. Height data, which demonstrate a clear increase in corrugation upon etching, are presented as Supporting Information (Figure S-2). Analyzing the PSD, we find a characteristic lateral distance of about 24 ± 5 nm (Figure 5e). This distance is larger than the molecular distance of ~15 nm, suggesting a possible lateral collapse of some P3HT domains after the removal of PLLA. (Since the P3HT is insoluble in the aqueous NaOH solution, longer scale mobility of these polymer chains is unlikely.) The fact that the PSD peak is not precisely twice that of the unetched film reflects an increase in the lateral disorder, which can also be seen in a broadening of the PSD spectrum. Studies on etching of a related polymer, poly(3-dodecylthiophene)-*b*-polylactide (P3DDT-*b*-PLA), were recently reported in the literature.[42] In that work, pits of various diameters and geometries, assumed to be due to phase separation which is dominated by crystallization of the rod block, were observed after etching. The gradual disappearance of peaks corresponding to PLLA allowed us to conclude that we have successfully removed the PLLA block from our structured films. We have created a morphology of vertically ordered P3HT domains separated by empty spaces and showing a characteristic distance in the range of the molecular dimension. XRD of the etched film still exhibits a diffraction peak corresponding to crystalline order, though the intensity is reduced. A second peak, centered at ~8.5°, may indicate regions in which there is greater interdigitation of the hexyl side chains and, hence, closer molecular spacing.

Some of the lateral collapse of the P3HT domains following etching may be the result of forces generated by the surface tension of the water in the drying film (~72 mN/m). In an effort to alleviate these forces, a solvent exchange with dry absolute ethanol (~22 mN/m) was performed prior to drying. AFM of the resulting film is depicted in Figure 5d, with the corresponding PSD in Figure 5e. Comparing to the PSD from the sample dried directly from water, it is clear that the solvent exchange resulted in somewhat larger percentage of periodicities with smaller scale, that is, closer to the original lamellar spacing. Ongoing experiments are aimed at optimizing this process.

Once the PLLA block has been removed, one can fill the empty spaces with electron acceptor material, such as C_{60}. This procedure has been performed by dip-coating thin films in an aqueous solution of the acceptor. Results are summarized in Figure 6a. The first spectrum (bottom, red line) was taken for a thin film of

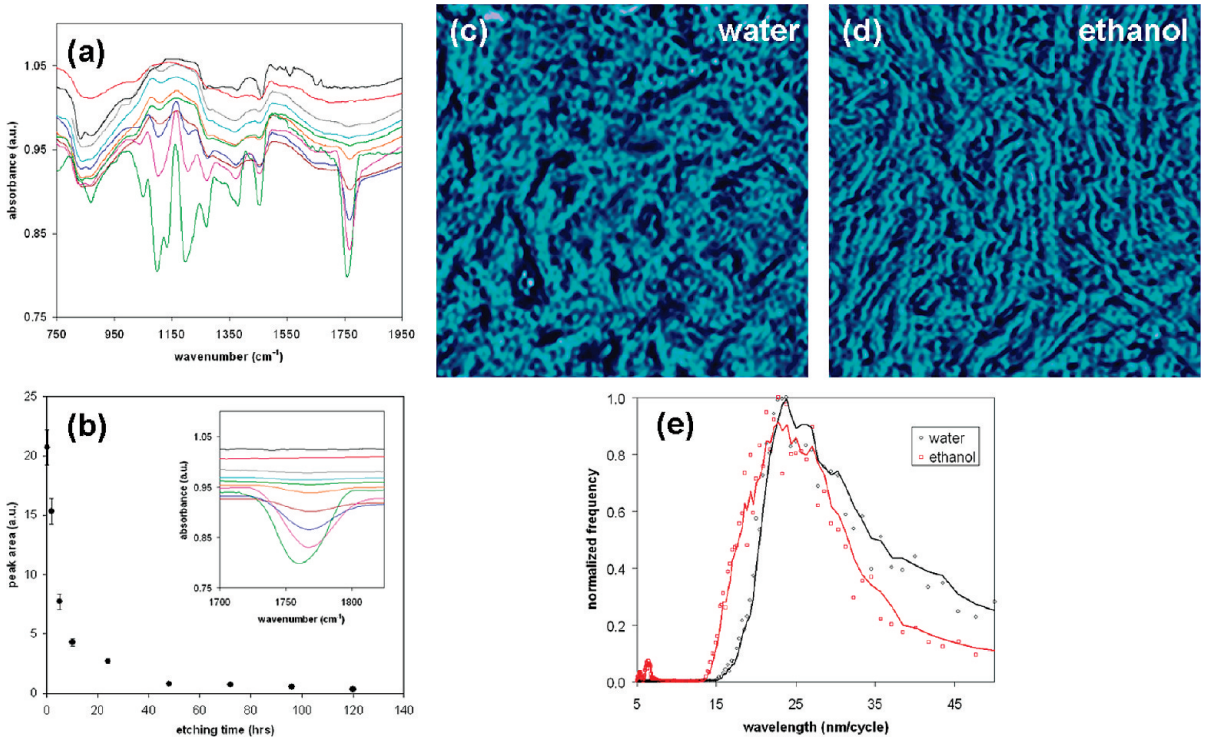

Figure 5. (a) ATR FT-IR spectra recorded for a thin film of P3HT homopolymer (first spectrum on top) and for several films of P3HT-*b*-PLLA which were etched in 0.5 M NaOH solution for 120, 96, 72, 48, 24, 10, 5, 2, and 0.25 h, respectively (the rest of spectra from top to bottom). (b) Decrease of PLLA peak located at 1765 cm^{-1} with the etching time. The inset highlights the decreasing peak. (c) TM-AFM phase image showing the morphology of a P3HT-*b*-PLLA thin film (69 ± 3 nm thickness) previously spin-cast from chloroform solution on ITO-covered glass and then etched for 5 days. (d) TM-AFM phase image showing the same preparation with the addition of an ethanol solvent exchange step prior to drying. (e) Corresponding PSD for (c) and (d). The peaks about 1095 and 1765 cm^{-1} are due to C−O−C and carbonyl stretching vibrations, respectively. Another peak about 1450 cm^{-1} was assigned to C−H stretching in methyl groups. The size of the AFM images is 1 μm^2.

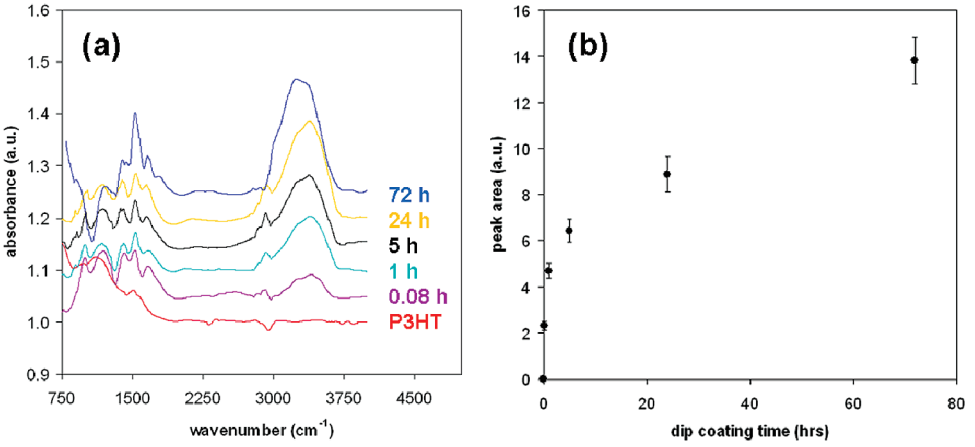

Figure 6. (a) ATR FT-IR spectra recorded for a thin film of P3HT homopolymer (first spectrum on bottom) and for several films of P3HT-*b*-PLLA which were etched for 5 days in 0.5 M NaOH solution and then dip-coated in aqueous solution of C_{60} (15 mg/mL, pH = 8.7) for 72, 24, 5, 1, and 0.08 h, respectively (the rest of spectra from bottom to top). (b) Increase of C_{60} peak located at 3360 cm^{-1} with the dip-coating time. All films were spin-cast from chloroform solution on ITO-covered glass.

P3HT homopolymer to serve as a reference with no C_{60} content. The rest of the spectra were recorded for etched films of P3HT-*b*-PLLA (thus containing just nanostructured P3HT material) which were dip-coated in C_{60} solution for times varying between 0.08 and 72 h.

An analysis of these ATR FT-IR spectra reveals that two peaks (1655 and 3360 cm^{-1}) increase with the dip-coating time. According to the FT-IR spectrum provided by the vendor (not shown), these two peaks are assigned to stretching vibrations of the C_{60} acceptor material. Figure 6b shows the increase of the C_{60} peak at 3360 cm^{-1} with the dip-coating time. These data demonstrate that C_{60} material was transferred to the nanostructured thin films of P3HT. AFM data following 72 h of dip-coating in 15 mg/mL solution (Figure S-3) also confirm the presence of fullerene on, and presumably within, the film. Because polar surface moieties of the C_{60} acceptor material do not possess an affinity for essentially nonpolar P3HT, it is likely that this material is located within the empty domains created after the removal of PLLA (as opposed to on top of the P3HT stripes). In order to detect C_{60} material in films using the ATR FT-IR technique, it is necessary to perform a minimum dip-coating time of about 0.08 h. Below this period of time, we could not detect any C_{60} material. When

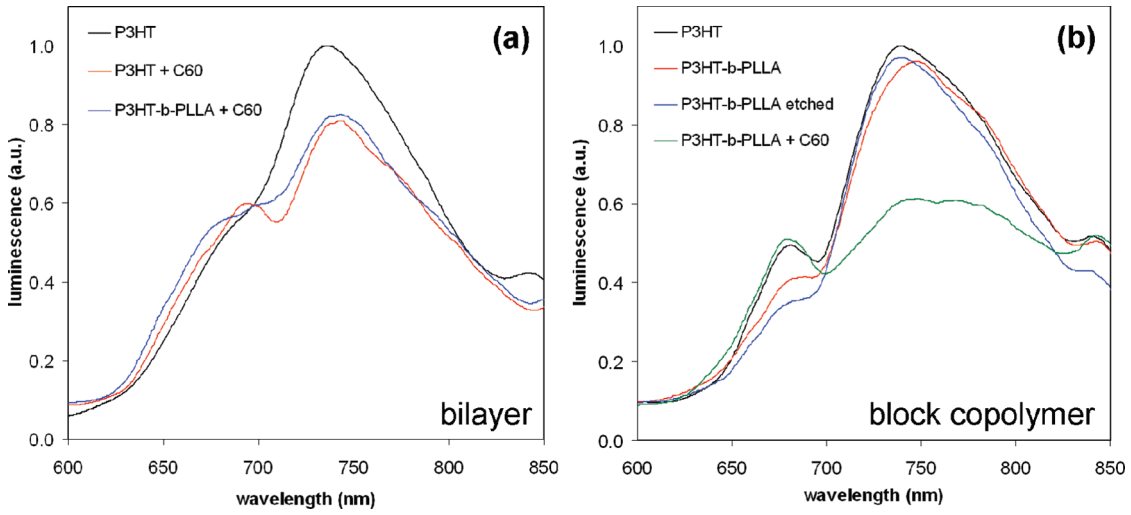

Figure 7. Photoluminescence spectra of (a) thin films of P3HT homopolymer and bilayers comprised of P3HT + C_{60} hydroxide and P3HT-*b*-PLLA + C_{60} hydroxide and (b) thin films of P3HT homopolymer, P3HT-*b*-PLLA before and after NaOH etching, and etched P3HT-*b*-PLLA filled with C_{60} hydroxide. The block copolymer film exhibits PL characteristic of P3HT both before and after etching. Substantial quenching is observed, however, upon filling with the electron-accepting material, suggesting that many excitons are being separated at the interfaces. Quenching with the block copolymer material is ~100% larger than with the simple bilayer construction. Excitation wavelength was 500 nm for all spectra.

dip-coating thin films for very long times, it is likely that too much C_{60} material is transferred, effectively overloading the former PLLA volume. As this particular form of C_{60} has not been used previously in optoelectronic systems, it is important to determine if it will indeed accept electrons from P3HT. Photoluminescence (PL) spectra can provide relevant information because P3HT has characteristic PL due to radiative exciton decay around 750 nm (Figure 7). For a baseline comparison, PL spectra were obtained from simple bilayer structures comprised of P3HT with C_{60} and of P3HT-*b*-PLLA with C_{60} (Figure 7a). Some quenching is observed due to electron transfer across the interface between the two stacked layers. This result implies that electrons can indeed be transferred from the polymer to the C_{60} molecules. The nanoporous film prepared using the block copolymer provides a significant enhancement of interfacial area available for transfer to the fullerene moieties and should, therefore, exhibit greater PL quenching. PL from the P3HT-*b*-PLLA film similar to P3HT is observed both prior to and after etching (Figure 7b). Following infiltration with the C_{60}, however, the PL spectrum exhibits significant, though not total, quenching. Compared to the simple bilayer film, this film exhibits about twice as much quenching. Incomplete quenching is likely a result of the presence of some domains larger than the exciton diffusion distance in P3HT that were formed by lateral collapse. As described above, optimizing the etching process may minimize or eliminate this collapse and therefore strengthen the PL quenching. Ongoing experiments will focus on fabrication of prototype solar energy devices and will establish the dip-coating time which is needed in order to transfer the optimum amount of C_{60} acceptor material. The traditional hole transport layer for organic PV, PEDOT:PSS, is not compatible with the processes described above, so studies on alternative materials having different solubility are currently being performed.

Conclusion

We have rationally designed a block copolymer and employed it both as a structure-directing agent and as an active material to create an idealized ordered morphology. Such morphology consisted of self-assembled alternating P3HT donor domains, with a periodicity approximately matching the molecular dimension, and C_{60} acceptor domains (Figure 1d). Using this intimate morphological control, we can now begin to probe structure−property relationships with unprecedented detail with the ultimate goal of maximizing the performance of future organic/hybrid PV devices.

Acknowledgment. Use of the Center for Nanoscale Materials was supported by the U.S. Department of Energy, Office of Science, Office of Basic Energy Sciences, under Contract DE-AC02-06CH11357.

Supporting Information Available: Differential scanning calorimetry data of P3HT-*b*-PLLA block copolymer (Figure S1); TM-AFM height images of the P3HT-*b*-PLLA (Figure S2); TM-AFM phase image of a nanostructured P3HT film infiltrated with C_{60}−OH (Figure S3). This material is available free of charge via the Internet at http://pubs.acs.org.

References and Notes

(1) King, R. R.; Law, D. C.; Edmondson, K. M.; Fetzer, C. M.; Kinsey, G. S.; Yoon, H.; Sherif, R. A.; Karam, N. H. *Appl. Phys. Lett.* **2007**, *90*, 183516.
(2) Thompson, B. C.; Fréchet, J. M. J. *Angew. Chem., Int. Ed.* **2008**, *47*, 58.
(3) Shaheen, S. E.; Brabec, C. J.; Sariciftci, N. S.; Padinger, F.; Fromherz, T.; Hummelen, J. C. *Appl. Phys. Lett.* **2001**, *78*, 841.
(4) Huynh, W. U.; Dittmer, J. J.; Alivisatos, A. P. *Science* **2002**, *295*, 2425.
(5) Kim, Y.; Cook, S.; Tuladhar, S. M.; Choulis, S. A.; Nelson, J.; Durrant, J. R.; Bradley, D. D. C.; Giles, M.; McCulloch, I.; Ha, C.-S.; Ree, M. *Nat. Mater.* **2006**, *5*, 197.
(6) Peumans, P.; Uchida, S.; Forrest, S. R. *Nature* **2003**, *425*, 158.
(7) Li, G.; Shrotriya, V.; Yao, Y.; Yang, Y. *J. Appl. Phys.* **2005**, *98*, 043704.
(8) Reyes-Reyes, M.; Kim, K.; Carroll, D. L. *Appl. Phys. Lett.* **2005**, *87*, 083506.
(9) Dai, J.; Jiang, X.; Wang, H.; Yan, D. *Appl. Phys. Lett.* **2007**, *91*, 253503.
(10) Mandoc, M. M.; Kooistra, F. B.; Hummelen, J. C.; Boer, B. d.; Blom, P. W. M. *Appl. Phys. Lett.* **2007**, *91*, 263505.
(11) Nogueira, A. F.; Lomba, B. S.; Soto-Oviedo, M. A.; Correia, C. R. D.; Corio, P.; Furtado, C. A.; Hummelgen, I. A. *J. Phys. Chem. C* **2007**, *111*, 18431.
(12) Shiga, T.; Takechi, K.; Motohiro, T. *Sol. Energy Mater. Sol. Cells* **2006**, *90*, 1849.
(13) Tepavcevic, S.; Darling, S. B.; Dimitrijevic, N. M.; Rajh, T.; Sibener, S. J. *Small* **2009**, *5*, 1776; DOI: 10.1002/smll.200900093.

(14) Gadisa, A.; Mammo, W.; Andersson, L. M.; Admassie, S.; Zhang, F.; Andersson, M. R.; Inganas, O. *Adv. Funct. Mater.* **2007**, *17*, 3836.
(15) Lindner, S. M.; Huttner, S.; Chiche, A.; Thelakkat, M.; Krausch, G. *Angew. Chem., Int. Ed.* **2006**, *45*, 3364.
(16) Brabec, C. J.; Sariciftci, N. S.; Hummelen, J. C. *Adv. Funct. Mater.* **2001**, *11*, 15.
(17) Salafsky, J. S.; Lubberhuizen, W. H.; Schropp, R. E. I. *Chem. Phys. Lett.* **1998**, *290*, 297.
(18) Padinger, F.; Rittberger, R. S.; Sariciftci, N. S. *Adv. Funct. Mater.* **2003**, *13*, 85.
(19) Yu, G.; Gao, J.; Hummelen, J. C.; Wudl, F.; Heeger, A. J. *Science* **1995**, *270*, 1789.
(20) Ma, W.; Yang, C.; Gong, X.; Lee, K.; Heeger, A. J. *Adv. Funct. Mater.* **2005**, *15*, 1617.
(21) Koetse, M. M.; Sweelssen, J.; Hoekerd, K. T.; Schoo, H. F. M.; Veenstra, S. C.; Kroon, J. M.; Yang, X.; Loos, J. *Appl. Phys. Lett.* **2006**, *88*, 083504.
(22) Halls, J. J. M.; Walsh, C. A.; Greenham, N. C.; Marseglia, E. A.; Friend, R. H.; Moratti, S. C.; Holmes, A. B. *Nature* **1995**, *376*, 498.
(23) Alam, M. M.; Jenekhe, S. A. *Chem. Mater.* **2004**, *16*, 4647.
(24) McDonald, S. A.; Konstantatos, G.; Zhang, S.; Cyr, P. W.; Klem, E. J. D.; Levina, L.; Sargent, E. H. *Nat. Mater.* **2005**, *4*, 138.
(25) Greenham, N. C.; Peng, X.; Alivisatos, A. P. *Phys. Rev. B* **1996**, *54*, 17628.
(26) Kwong, C. Y.; Djurisic, A. B.; Chui, P. C.; Cheng, K. W.; Chan, W. K. *Chem. Phys. Lett.* **2004**, *384*, 372.
(27) Yang, X.; Loos, J. *Macromolecules* **2007**, *40*, 1353.
(28) Gunes, S.; Neugebauer, H.; Sariciftci, N. S. *Chem. Rev.* **2007**, *107*, 1324.
(29) van Duren, J. K. J.; Yang, X.; Loos, J.; Bulle-Lieuwma, C. W. T.; Sieval, A. B.; Hummelen, J. C.; Janssen, R. A. J. *Adv. Funct. Mater.* **2004**, *14*, 425.
(30) Sun, S.-S. *Sol. Energy Mater. Sol. Cells* **2003**, *79*, 257.
(31) Darling, S. B. *J. Phys. Chem. B* **2008**, *112*, 8891.
(32) Sommer, M.; Lindner, S. M.; Thelakkat, M. *Adv. Funct. Mater.* **2007**, *17*, 1493.
(33) Chen, X. L.; Jenekhe, S. A. *Macromolecules* **1996**, *29*, 6189.
(34) Tu, G.; Li, H.; Forster, M.; Heiderhoff, R.; Balk, L. G.; Scherf, U. *Macromolecules* **2006**, *39*, 4327.
(35) Zhang, Q.; Cirpan, A.; Russell, T. P.; Emrick, T. *Macromolecules* **2009**, *42*, 1079.
(36) Liang, Y.; Wang, H.; Yuan, S.; Lee, Y.; Gan, L.; Yu, L. *J. Mater. Chem.* **2007**, *17*, 2183.
(37) Barrau, S.; Heiser, T.; Richard, F.; Brochon, C.; Ngov, C.; van de Wetering, K.; Hadziioannou, G.; Anokhin, D. V.; Ivanov, D. A. *Macromolecules* **2008**, *41*, 2701.
(38) Hiorns, R. C.; Iratcabal, P.; Begue, D.; Khoukh, A.; de Bettignies, R.; Leroy, J.; Firon, M.; Sentein, C.; Martinez, H.; Preud'homme, H.; Dagron-Lartigau, C. *J. Polym. Sci., Part A: Polym. Chem.* **2009**, *47*, 2304.
(39) Sun, S.-S.; Zhang, C.; Ledbetter, A.; Choi, S.; Seo, K.; Bonner, C. E.; Drees, M.; Sariciftci, N. S. *Appl. Phys. Lett.* **2007**, *90*, 043117.
(40) Darling, S. B. *Prog. Polym. Sci.* **2007**, *32*, 1152.
(41) Darling, S. B. *Energy Environ. Sci.* **2009**, DOI: 10.1039/B912086F.
(42) Boudouris, B. W.; Frisbie, C. D.; Hillmyer, M. A. *Macromolecules* **2008**, *41*, 67.
(43) Sirringhaus, H.; Tessler, N.; Friend, R. H. *Science* **1998**, *280*, 1741.
(44) Shrotriya, V.; Ouyang, J.; Tseng, R. J.; Li, G.; Yang, Y. *Chem. Phys. Lett.* **2005**, *411*, 138.
(45) Halls, J. J. M.; Pichler, K.; Friend, R. H.; Moratti, S. C.; Holmes, A. B. *Appl. Phys. Lett.* **1996**, *68*, 3120.
(46) Thanki, P. N.; Dellacherie, E.; Six, J.-L. *Appl. Surf. Sci.* **2006**, *253*, 2758.
(47) Park, S. H.; Roy, A.; Beaupre, S.; Cho, S.; Coates, N.; Moon, J. S.; Moses, D.; Leclerc, M.; Lee, K.; Heeger, A. J. *Nat. Photonics* **2009**, *3*, 297.
(48) Kline, R. J.; McGehee, M. D.; Kadnikova, E. N.; Liu, J.; Fréchet, J. M. J.; Toney, M. F. *Macromolecules* **2005**, *38*, 3312.
(49) Dove, A. P. *Chem. Commun.* **2008**, *48*, 6446.
(50) Dai, C.-A.; Yen, W.-C.; Lee, Y.-H.; Ho, C.-C.; Su, W.-F. *J. Am. Chem. Soc.* **2007**, *129*, 11036.
(51) Heiser, T.; Adamopoulos, G.; Brinkmann, M.; Giovanella, U.; Ould-Saad, S.; Brochon, C.; van de Wetering, K.; Hadziioannou, G. *Thin Solid Films* **2006**, *511−512*, 219.
(52) Olsen, B. D.; Alcazar, D.; Krikorian, V.; Toney, M. F.; Thomas, E. L.; Segalman, R. A. *Macromolecules* **2008**, *41*, 58.
(53) Chen, T.-A.; Wu, X.; Rieke, R. D. *J. Am. Chem. Soc.* **1995**, *117*, 233.